high-temperature region near upstream of the main normal injection location. This region forms a continuous high-temperature area, the effect of which resembles that of a sparkplug in helping initializing and holding the main flame. Igniting the main fuel injected leads to the second increase of the upper-wall temperature, reaching its peak downstream of the injection station. The flow expansion caused by the 3-deg combustor divergence reduces the temperature towards the combustor exit. Other results for this case study are presented in Ref. 10.

The flowfield features are presented in Figs. 3 and 4. The velocity vectors plot with the superimposed streamlines are depicted at two crossflow locations. Figure 3 shows the vectors in the cavity region downstream of the pilot injection at $X = 40$ mm. The vectors at the main injection location, $X = 70$ mm, are shown in Fig. 4. The two plots exhibit the interaction between the incoming supersonic airflow and the pilot and main ethylene injections. The recirculations formed in the cavity are caused by the expansion effect of the step. The parallel pilot injections intensify the recirculations pattern in the cavity. This can be observed in Fig. 3 at the pilot injection location, $Y = 30.5$ mm. Figure 4 shows the interaction between the incoming supersonic airflow and the vortices formed as a result of the normal injection. This effect is manifested by observing the two counterflows at the midcombustor span, $Y \sim 15$ mm. The confrontation of the two counterflows is presented by the two loops in the streamlines around $Z = \pm 0.0065$ m. The counterflow has the effect of increasing the diffusion between the fuel and air and eventually enhancing the fuel/air mixing. The vortices formed around the fuel injection areas help in promoting the air-fuel mixing process and consequently lead to more efficient combustion.

Conclusions

The step plays a remarkable role in enhancing the fuel/air mixing. The pilot flame stabilizes and supports the main flame formed by the main vertical injection. The existence of the wedge downstream of the rearward-facing step helps in initiating and stabilizing the main flame. Work is underway to analyze the effect of the gaseous hydrogen pilot injection on the combustion of the sonic normal ethylene flow.

Acknowledgments

This work was supported, in part, by the Old Dominion University's Institute for Scientific and Educational Technology through NASA Langely Research Center, Cooperative Agreement NCC1-349. The cooperative agreement was monitored by Samuel E. Massenberg, Director, Office of Education.

References

[1]Northam, G. B., "Workshop Report: Combustion in Supersonic Flow," *21st JANNAF Combustion Meeting*, Oct. 1984.

[2]Kay, I. W., Chiappetta, L., and McVey, J. B., "Hydrocarbon-Fueled Scramjet, Combustor Investigation," Technical Rept. AFAPL-TR-68-146, Vol. IV, May 1969.

[3]Kay, I. W., McVey, J. B., Kepler, C. E., and Chiappetta, L., "Hydrocarbon-Fueled Scramjet, Piloting and Flame Propagation Investigation, Combustor Investigation," Technical Rept. AFAPL-TR-68-146, Vol. IX, May 1971.

[4]Northam, G. B., and Anderson, G. Y., "Supersonic Combustion Ramjet Research at Langley," AIAA Paper 86-0159, Jan. 1986.

[5]Westbrook, C. K., and Dryer, F. L., "Chemical Kinetics Modeling of Hydrocarbon Combustion," *Progress in Energy and Combustion Science*, Vol. 10, 1984, pp. 1–57.

[6]*Fluent Version 5.0 User's Guide*, Fluent, Inc., Lebanon, New Hampshire, 1998.

[7]McDaniel, J., Fletcher, D., Hartfield, R., and Hollo, S., "Staged Transverse Injection into Mach 2 Flow Behind a Rearward-Facing Step: A 3-D Compressible Test Case for Hypersonic Combustor Code Validation," AIAA Paper 91-5071, Dec. 1991.

[8]Taha, A. A., Tiwari, S. N., and Mohieldin, T. O., "Validation of Fluent CFD Code in Supersonic Flow Fields," AIAA Paper 2001-2637, June 2001.

[9]Owens, M., Segal, C., and Auslender, A. H., "Effects of Mixing Schemes on Kerosene Combustion in a Supersonic Air Stream," *Journal of Propulsion and Power*, Vol. 13, No. 4, 1997, pp. 525–531.

[10]Taha, A. A., Tiwari, S. N., and Mohieldin, T. O., "Numerical Simulation of Ignition/Combustion Characteristics of Ethylene in Supersonic Air Streams," AIAA Paper 2000-3584, July 2000.

High-Intensity Sound Absorption at an Orifice with Bias Flow

Xiaodong Jing* and Xiaofeng Sun†
Beijing University of Aeronautics and Astronautics, Beijing 100083, People's Republic of China

I. Introduction

A PERFORATED liner has been widely used to control noise or suppress combustion instability in the afterburner of a jet engine or the combustor of a rocket engine. For the suppression of combustion instability, cooling air is introduced through the orifices to protect the liner from being burnt. Previous research[1] showed that mean bias flow also enhances the sound absorption at an orifice. It was further proposed that bias flow could be employed to control the liner impedance, thereby greatly increasing the duct attenuation.[2] Various models[3,4] have been set up to study the bias flow effect on the orifice impedance. A common feature of the preceding models is that the incident sound is assumed to be of low intensity and to interact linearly with mean bias flow. On the other hand, considerable research[1,4–7] has been carried out on the nonlinear sound dissipation at an orifice in the absence of mean flow, and it was shown that the velocity of the sound-excited oscillatory flow in the orifice could be very large at high sound pressure levels. Thus, in the situation of high-intensity sound incident on an orifice with bias flow, there will be little evidence for assuming linear flow–acoustic interaction. To the authors' knowledge, there has been experimental investigations[8] on the combining effect of mean bias flow and high sound intensity on the orifice impedance, but the related theoretical studies are very few.

Previous studies have provided persuasive evidence that the sound absorption that occurs at an orifice is due to the conversion of the acoustic energy into vortical energy, either in the presence of mean bias flow[3] or at high sound intensity.[4–7] It is reasonable to believe that this mechanism is also applied to the high-intensity sound absorption at an orifice in the presence of bias flow. From this point of view, we first employ a discrete vortex model to simulate the vortex shedding process produced by high-intensity sound at an orifice with bias flow. This model is also used to obtain some quantitative results, including the average velocity through the orifice and the orifice acoustic impedance. In addition, a quasi-steady model is further developed to study this phenomenon.

II. Theoretical Models

Consider the phenomenon that a low-frequency, high-amplitude sinusoidal sound is incident on a circular orifice of radius R that is located in an infinitely thin, rigid plate. There is also mean bias flow through the orifice. The total pressure difference Δp across the orifice plate can be written as follows:

$$\Delta p = P_B + P_A \cos(\omega t) \tag{1}$$

where P_B is steady pressure difference producing bias flow, P_A is the amplitude of the incident sound, ω is angular frequency, and t is time.

A. Discrete Vortex Model

The discrete vortex model of Ref. 6 is modified to study the sound-excited vortex shedding at the orifice. To obtain a smooth

Received 16 March 2001; revision received 20 October 2001; accepted for publication 20 November 2001.

*Associate Professor, Department of Jet Propulsion.
†Professor, Department of Jet Propulsion. AIAA Member.

roll-up of the vortex sheet within relatively long computing time, a vortex-blob smoothing parameter δ is introduced to suppress the short-wavelength Helmholtz instability as proposed by Nitsche and Krasny[9]; δ is time dependent and given as

$$\delta = \varepsilon\sqrt{t}H(\delta_m - \delta) + \delta_m H(\delta - \delta_m) \tag{2}$$

where $H(x)$ is the Heaviside function, ε is a select factor, and δ_m is a select maximum value of δ. Note that the analytical method developed in Ref. 6 for computing the flowfield around an orifice is accurate only for $\delta = 0$. However, for the discrete vortex rings near the orifice, the vortex-blob smoothing parameter δ given by Eq. (2) is so small that the flowfield can still be computed by the analytical method to a good approximation.

B. Analytical Model

Based on the quasi-steady assumption, the pressure drop across the orifice plate can be approximately related to the flow velocity through the orifice using the Bernoulli equation

$$\Delta p = \rho_0 u^2 \big/ 2C_v^2 \tag{3}$$

where ρ_0 is air density. C_v is the well-known vena contracta coefficient taken to be 0.61 in this Note. The following nondimensional variables are introduced:

$$\lambda = P_A/P_B, \qquad \bar{L} = L/R, \qquad \Delta\bar{p} = \Delta p/P_B$$

$$\bar{u} = u\sqrt{\rho_0/P_B}, \qquad \bar{t} = t\sqrt{P_B/\rho_0 R^2}$$

Then, the average velocity though the orifice can be obtained from Eqs. (1) and (3),

$$\bar{u} = \mathrm{sgn}(1 + \lambda\cos Sr\bar{t})C_v\sqrt{2|1 + \lambda\cos Sr\bar{t}|} \tag{4}$$

where $Sr = \omega R\sqrt{(\rho_0/P_B)}$ is the Strouhal number. The Fourier decomposition of u can be expressed as follows:

$$\bar{u}(\bar{t}) = \bar{U}_0 + \sum_{n=1}^{\infty} \bar{U}_n \cos(nSr\bar{t}) \tag{5}$$

Computation indicates that the first harmonic amplitude is always 10 dB higher than the second, or 16 dB higher than the third. This provides evidence to define the acoustic impedance of an orifice in terms of the first harmonic of the average velocity. In this Note, the acoustic impedance of an orifice is normalized by $\sqrt{(\rho_0 P_B)}$; thereby, it can be expressed as function of only two nondimensional parameters, λ and Sr. The normalized specific acoustic resistance of the orifice is given as

$$z_r = \lambda/\bar{U}_1 \tag{6}$$

where

$$\bar{U}_1(\lambda) = \frac{2}{\pi}\int_0^{+\pi} \mathrm{sgn}(1 + \lambda\cos y)\sqrt{2|1 + \lambda\cos y|}\cos y\,\mathrm{d}y$$

The integration in the preceding equation is numerically carried out. This method is basically an extension of Cummings and Eversman's[4] model of high-intensity sound effects.

III. Results and Discussion

When $Sr = 0.707$ and $\lambda = 1.0$, the development of the sound-excited orifice flow is given in Figs. 1a–1d. The start vortex of bias flow appears at the very beginning of the cycle (Fig. 1a). As time increases, a second rolled up vortex structure is formed due to the excitation of high-intensity incident sound, as shown in Fig. 1c. Vortex shedding has been observed in experiment[5] or numerical simulations[6,7] when high-intensity sound was incident on an orifice in the absence of mean flow. The present simulation demonstrates that, in the presence of bias flow, strong vortex shedding also occurs at an orifice when the incident sound intensity is very high,

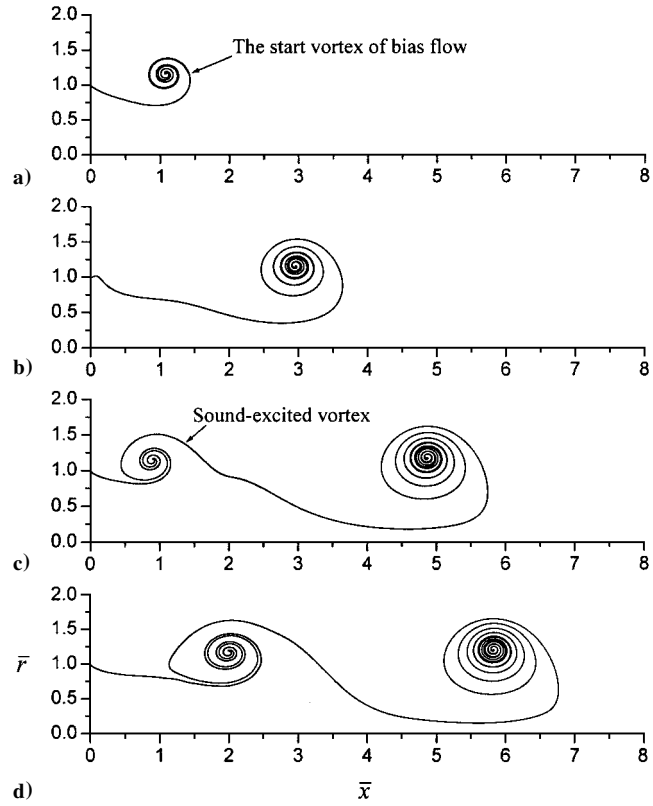

Fig. 1 Development of the orifice flow under the excitation of high-intensity sound for $\lambda = 1.0$ and $Sr = 0.71$: a) $\bar{t} = 2.09$, b) $\bar{t} = 4.19$, c) $\bar{t} = 6.28$, and d) $\bar{t} = 7.33$.

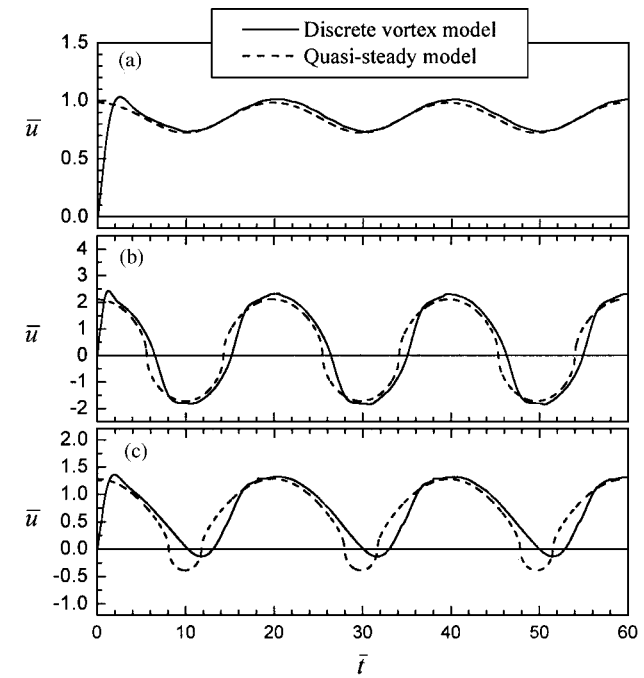

Fig. 2 Time history of average velocity through the orifice for $Sr = 0.32$: a) $\lambda = 0.2$, b) $\lambda = 5.0$, and c) $\lambda = 1.2$.

thereby resulting in substantial acoustic absorption. Figure 2 gives the time history of the average velocity through the orifice for different values of λ when $Sr = 0.32$. It is shown that the discrete vortex model is generally in good agreement with the quasi-steady method. When λ has a small value, bias flow velocity is much larger than the fluctuating velocity amplitude, as shown in Fig. 2a. The spectrum analysis for the results in Fig. 2a shows that U_1 is 26 times as large as U_2, and it is about 370 times larger than U_3. Thus, in this case, the

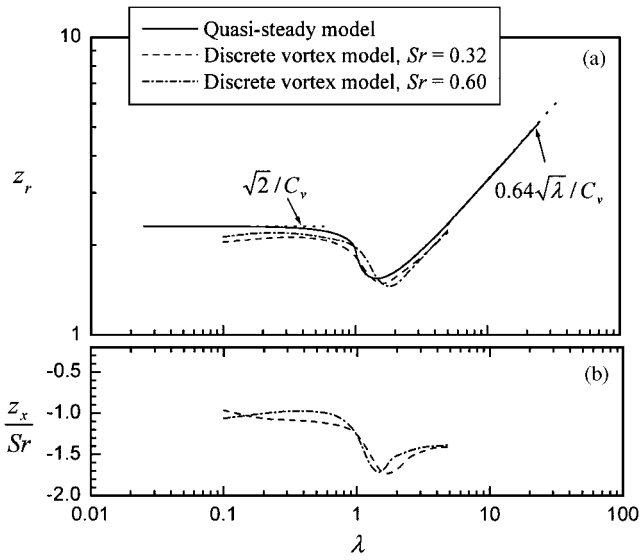

Fig. 3 Normalized specific acoustic impedance plotted as a function of the nondimensional sound pressure amplitude: a) resistance and b) reactance.

fluctuating velocity through the orifice is essentially sinusoidal; no marked distortion appears in the velocity curve. As the normalized sound pressure amplitude increases to 5.0, the fluctuating velocity amplitude is far larger than bias flow velocity (Fig. 2b). It can also be seen that, due to the nonlinear effect, the velocity curve has been distorted. Further computation indicates that U_1 is about 10 times as large as U_2 or U_3. Compared with the case of $\lambda = 0.3$, the amplitudes of the higher harmonics have been greatly increased. When λ is near unity, the flow in the orifice is in a transition state between the two cases mentioned, and the effect of sound intensity is comparable to that of mean flow, as shown in Fig. 2c. We can see that, in this transition state, the flow velocity distortion is very severe. The spectrum analysis for the flow velocity in Fig. 2c shows that U_1 is only four times as large as U_2.

In Fig. 3a, z_r is plotted as a function of λ. We can see that the results of the discrete vortex model for two different Strouhal numbers nearly coincide and agree well with the quasi-steady model. Figure 3 shows that, in terms of the variation of the acoustic resistance, there exist three different regions. In region 1 where $\lambda < 0.6$, the fluctuating velocity amplitude is far smaller than bias flow velocity; thus, z_r has a constant value of $\sqrt{(2)}/C_v$. In contrast in region 3, where $\lambda > 3.0$, the high sound intensity effect dominates; thereby z_r approaches the equation $0.64\sqrt{(\lambda)}/C_v$, which is obtained from the model of Ref. 4. In region 2, where $0.6 < \lambda < 3.0$ (correspondingly the ratio of the fluctuating velocity amplitude to bias flow velocity is between 0.3 and 4.0), the orifice flow is in a transition state between regions 1 and 3. In this region, the normalized acoustic resistance is smaller than $\sqrt{(2)}/C_v$ and decreases to about 70% of this value at the lowest point. This decrease of z_r is probably due to the considerable reduction of the average velocity during the negative half cycle, as shown in Fig. 2c. One advantage of the discrete vortex model over the quasi-steady model is in the prediction of the acoustic reactance. The computed acoustic reactance is shown in Fig. 3b. The numerical results indicate that the normalized specific acoustic reactance is in proportional to the Strouhal number Sr; thus, z_x/Sr is only the function of λ. This means that the inertance of the orifice only depends on the nondimensional sound pressure amplitude.

IV. Conclusions

A discrete vortex model and a quasi-steady method are employed to study high-intensity sound absorption at an orifice with bias flow. Generally, good agreement is obtained between the two methods. The numerical simulation demonstrates that, in the presence of bias flow, strong vortex shedding also occurs at an orifice when the incident sound intensity is very high, thereby resulting in substantial acoustic absorption. It is also shown that, when the ratio of the fluctuating velocity amplitude to bias flow velocity is within the range from 0.3 to 4.0, the orifice flow is in a transition state between the two limit cases dominated by bias flow and high sound intensity, respectively. In this region, a decrease of the acoustic resistance is seen as the sound pressure amplitude increases. One advantage of the discrete vortex model over the quasi-steady method is in the prediction of the orifice acoustic reactance. The numerical computation indicates that the inertance of the orifice depends on the ratio between the sound pressure amplitude and the steady pressure difference producing bias flow.

Acknowledgments

This work is sponsored by the National Natural Science Foundation of the People's Republic of China (59925616) and the Aeronautical Science Foundation of the People's Republic of China (00C51040).

References

[1] Ingard, U., and Ising, H., "Acoustic Nonlinearity of an Orifice," *Journal of the Acoustical Society of America*, Vol. 42, No. 2, 1967, pp. 6–17.

[2] Dean, P. D., and Tester, B. J., "Duct Wall Impedance Control as an Advanced Concept for Acoustic Suppression," NASA CR-134998, 1975.

[3] Howe, M. S., "On the Theory of Unsteady High Reynolds Number Flow Through a Circular Aperture," *Proceedings of the Royal Society of London*, Vol. A366, No. 1724, 1979, pp. 205–223.

[4] Cummings, A., and Eversman, W., "High Amplitude Acoustic Transmission Through Duct Terminations: Theory," *Journal of Sound and Vibration*, Vol. 91, No. 4, 1983, pp. 503–518.

[5] Salikuddin, M., and Ahuja, K. K., "Acoustic Power Dissipation on Radiation Through Duct Terminations: Experiment," *Journal of Sound and Vibration*, Vol. 91, No. 4, 1983, pp. 479–502.

[6] Jing, X., and Sun, X., "Discrete Vortex Simulation on the Acoustic Nonlinearity of an Orifice," *AIAA Journal*, Vol. 38, No. 9, 2000, pp. 1565–1572.

[7] Tam, C. K. W., Kurbatski, K. A., Ahuja, K. K., Jr., and Gaeta, R. G., "Numerical Investigation of the Dissipation Mechanism of Resonant Acoustic Liners," AIAA Paper 2001-2262, May 2001.

[8] Salikuddin, M., Syed, A. A., and Mungur, P., "Acoustic Characteristics of Perforated Sheets with Throughflow in a High Intensity Noise Environment," *Journal of Sound and Vibration*, Vol. 169, No. 2, 1994, pp. 145–177.

[9] Nitsche, M., and Krasny, R., "A Numerical Study of Vortex Ring Formation at the Edge of a Circular Tube," *Journal of Fluid Mechanics*, Vol. 276, 1994, pp. 139–161.